ISSN 0001-4338, Izvestiya, Atmospheric and Oceanic Physics, 2017, Vol. 53, No. 2, pp. 174–186. © Pleiades Publishing, Ltd., 2017.
Original Russian Text © N.V. Vazaeva, O.G. Chkhetiani, R.D. Kouznetsov, M.A. Kallistratova, V.F. Kramar, V.S. Lyulyukin, D.D. Kuznetsov, 2017, published in Izvestiya Rossiiskoi Akademii Nauk, Fizika Atmosfery i Okeana, 2017, Vol. 53, No. 2, pp. 200–214.

Estimating Helicity in the Atmospheric Boundary Layer from Acoustic Sounding Data

N. V. Vazaeva[a, b, *], O. G. Chkhetiani[a, c], R. D. Kouznetsov[a, d], M. A. Kallistratova[a], V. F. Kramar[a], V. S. Lyulyukin[a], and D. D. Kuznetsov[a]

[a] *Obukhov Institute of Atmospheric Physics, Russian Academy of Sciences, Moscow, 119017 Russia*
[b] *Bauman Moscow State Technical University, Moscow, 105005 Russia*
[c] *Space Research Institute, Russian Academy of Sciences, Moscow, 117997 Russia*
[d] *Finnish Meteorological Institute, FI-00101, Helsinki, Finland*
**e-mail: ifanataly@gmail.com*

Received December 22, 2015; in final form, March 18, 2016

Abstract—Distributions of the velocity-field helicity in the atmospheric boundary layer have been obtained from acoustic sounding data. The helicity of large-scale motions (0.3–0.6 m/s^2) exceeds (by an order of magnitude) its independently measured turbulent values, which are close to helicity averaged over the layer (0.02–0.12 m/s^2). In the absence of strong convection, there is good correlation between helicity and wind velocity squared at upper sounding levels of 400 to 600 m.

Keywords: ABL, acoustic sounding, numerical simulation, helicity

DOI: 10.1134/S0001433817020104

INTRODUCTION

Since the 1950s, special interest has been expressed in mesoscale circulation in the atmospheric boundary layer (ABL) and its characteristic manifestations, in particular, such as quasiperiodic roll structures—ordered helical vortices (rolls) with horizontal axes [1, 2]. Such long-lived vortices are formed at a sufficiently weak wind of 2–3.5 m/s [3], when three-dimensional convective cells are transformed into longitudinally oriented ones, and they are well visualized in the form of the so-called cloud streets that are clearly visible in satellite images [4]. Their horizontal scales amount to 3–5 km [3].

In the ABL, mesoscale-circulation structures affect the characteristics of turbulence, form mean-flow profiles, and play a significant part in mixing processes and processes of transport of humidity, heat, and other substances through the ABL into the free atmosphere. According to estimates obtained in [5–7], secondary airflows in the form of roll structures are responsible for 20–60% of the total heat-mass transfer through the ABL.

One significant characteristic of coherent structures in the ABL is helicity—a scalar product of velocity field and vorticity [8]:

$$H = \mathbf{v}\,\mathrm{rot}(\mathbf{v}).$$

In the ABL, large-scale flows, whose structure is determined by combined effects of turbulent friction and the Coriolis force, have a nonzero helicity [9–11]. Correspondingly, turbulent motions in the ABL are characterized by a nonzero helicity [12], which has been supported by results obtained from field experiments carried out by the Obukhov Institute of Atmospheric Physics (IAP) [13, 14] and direct numerical simulation (DNS) [15]. Helicity has attracted particular interest because of its role in the genesis and dynamics of large-scale atmospheric and oceanic motions [16], advantages due to the parameterization of its dynamic effect in mesoscale ABL models [17], and its possible use as a prognostic factor [18].

In order to obtain data on helicity, it is necessary to know spatial wind-velocity distributions.

Results obtained (in IAP experiments) from the acoustic sounding of the ABL over arid-steppe zones in southern Russia (Chernozemelskii raion, Republic of Kalmykia, 2007) [3], the Tsimlyansk Scientific Station (2012) [14], and Spitsbergen (2009) [19] have been analyzed in this study. Profiles of the wind-velocity components at heights of 400–600 m (up to 100 m for Spitsbergen) with a step of 10–30 m and a time resolution of 5–10 s have been obtained from observational data. The spatial distribution of helicity and its time variations have been calculated and compared to theoretical estimates and calculations based on a WRF-ARW mesoscale atmospheric model.

1. HELICAL FLOWS IN THE EKMAN BOUNDARY LAYER

The velocity-field components for the Ekman flow with no-slip conditions at the lower boundary have the form

$$U(z) = U_G\left(1 - \exp\left(-\frac{z}{h}\right)\cos\frac{z}{h}\right) - V_G\exp\left(-\frac{z}{h}\right)\sin\frac{z}{h}, \quad (1)$$

$$V(z) = V_G\left(1 - \exp\left(-\frac{z}{h}\right)\cos\frac{z}{h}\right) + U_G\exp\left(-\frac{z}{h}\right)\sin\frac{z}{h}. \quad (2)$$

Here, $h = \sqrt{K/\Omega}$ is the Ekman scale, Ω is the frequency of external rotation (Earth rotation), V_G and U_G are the components of geostrophic wind velocity in the free atmosphere, z is the vertical coordinate, and K is the turbulent viscosity coefficient introduced by analogy with kinematic viscosity. Such an approach is widely used in solving the Ekman equations, studying stability problems [8, 20], and analyzing mesoscale motions in the ABL [21].

In this case, the helicity is determined only by the horizontal vorticity components and has the form [8, 10, 11]

$$H(z) = -U(z)\frac{\partial V}{\partial z} + V(z)\frac{\partial U}{\partial z}. \quad (3)$$

Substituting (1) and (2) into (3) gives (for the vertical helicity distribution) [8]:

$$H(z) = u_g^2 h^{-1}\left\{\exp\left(-\frac{z}{h}\right)\left(\sin\frac{z}{h} - \cos\frac{z}{h}\right) + \exp\left(-\frac{2z}{h}\right)\right\},$$

here, $u_g^2 = U_G^2 + V_G^2$.

Hence, upon integrating over the vertical coordinate, we obtain that integral helicity H_{int} is exactly 1/2 of the geostrophic-wind velocity squared [10]:

$$H_{\text{int}} = \int_0^\infty H(z)dz = \frac{1}{2}(U_G^2 + V_G^2). \quad (4)$$

With consideration for the real structure of the turbulent ABL under different stratifications, integral helicity will differ from that in (4). Nevertheless, Eq. (4) may be used as an assessment of integral helicity and, as is shown below, adequately reflects its temporal dynamics.

In addition, let us give integral helicity values for simple modifications of the Ekman profile, which already provide a turning-angle decrease when compared to an Ekman value of 45°.

When the contribution of turbulent helicity to Reynolds stresses is taken into account [12],

$$H_{\text{int}} = \frac{1}{2}(U_G^2 + V_G^2)((1 + g^2)^{1/2} - g),$$

where g ~ 0.1–0.3 characterizes turbulent helicity. For the Taylor solution [22], in which the slip conditions $\frac{\partial U(V)}{\partial z} = \lambda U(V)$, where $\lambda = \frac{1}{\epsilon H}$, are considered at the lower boundary, we have for integral helicity

$$H_{\text{int}} = \frac{(U_G^2 + V_G^2)}{2\left(1 + \frac{2\epsilon^2}{2\epsilon + 1}\right)}.$$

2. INSTRUMENATION AND MEASUREMENT CONDITIONS

In all the experiments mentioned in the Introduction, the vertical profiles of the wind-velocity components were measured using atmospheric acoustic sounding. Acoustic sounders—sodars—appeared in the 1970s due to A.M. Obukhov's ideas of using the phenomenon of sound scattering from small-scale turbulent inhomogeneities in atmospheric studies [23]. The reliability and accuracy of sodar measurements have been studied for many years [24]. At present, acoustic sounding is a well-tested method of studying the lower ABL [25, 26] used widely all over the world [27, 28].

Doppler three-component monostatic sodars (LATAN-3M) and minisodars (LATAN-3m) with a frequency encoded sounding pulse, which were developed and manufactured at the IAP, were used to measure vertical profiles of the three wind-velocity components [3, 29, 30].

(1) Sodar measurements were performed over the Caspian Lowland (Kalmykia) in the vicinity of the village of Komsomolskii to the south of the Chernye Zemli Nature Reserve from July 21 to August 1, 2007. Three spaced sodars were combined into one network using radiotelephones and were synchronized according to signals from GPS satellites [3]. A longwave LATAN-3M sodar with a vertical resolution of 30 m, a pulse emission interval of 10 s, an altitude range of 800 m, and a basic carrier frequency of 2 kHz was used to estimate the vertical extent of upward convective airflows. The three minisodars with a vertical resolution of 20 m, a pulse emission interval of 5 s, an altitude range of 400 m, and a basic carrier frequency of 3.5 kHz were located at the vertexes of a triangle with its side lengths of 3.5, 1.4, and 3.2 km. Such a configuration made it possible to estimate the horizontal scales of convective motions and details of the spatial structure of vortex coherent formations.

(2) Within a period of August 2–26, 2012, sodar measurements were performed at the IAP Tsimlyansk Scientific Station simultaneously with measurements described in detail in [14]. A LATAN-3m minisodar with an improved vertical resolution of 10 m was used.

(3) Within a period of May 3–13, 2009, measurements were performed on the island of Spitsbergen. Sodars were located on the Kongsvegen glacier [19]. Two LATAN-3m minisodars were used.

These measurements were continuously performed. The time variations in vertical-velocity distributions for Kalmykia and Tsimlyansk (see, for example, Fig. 5)

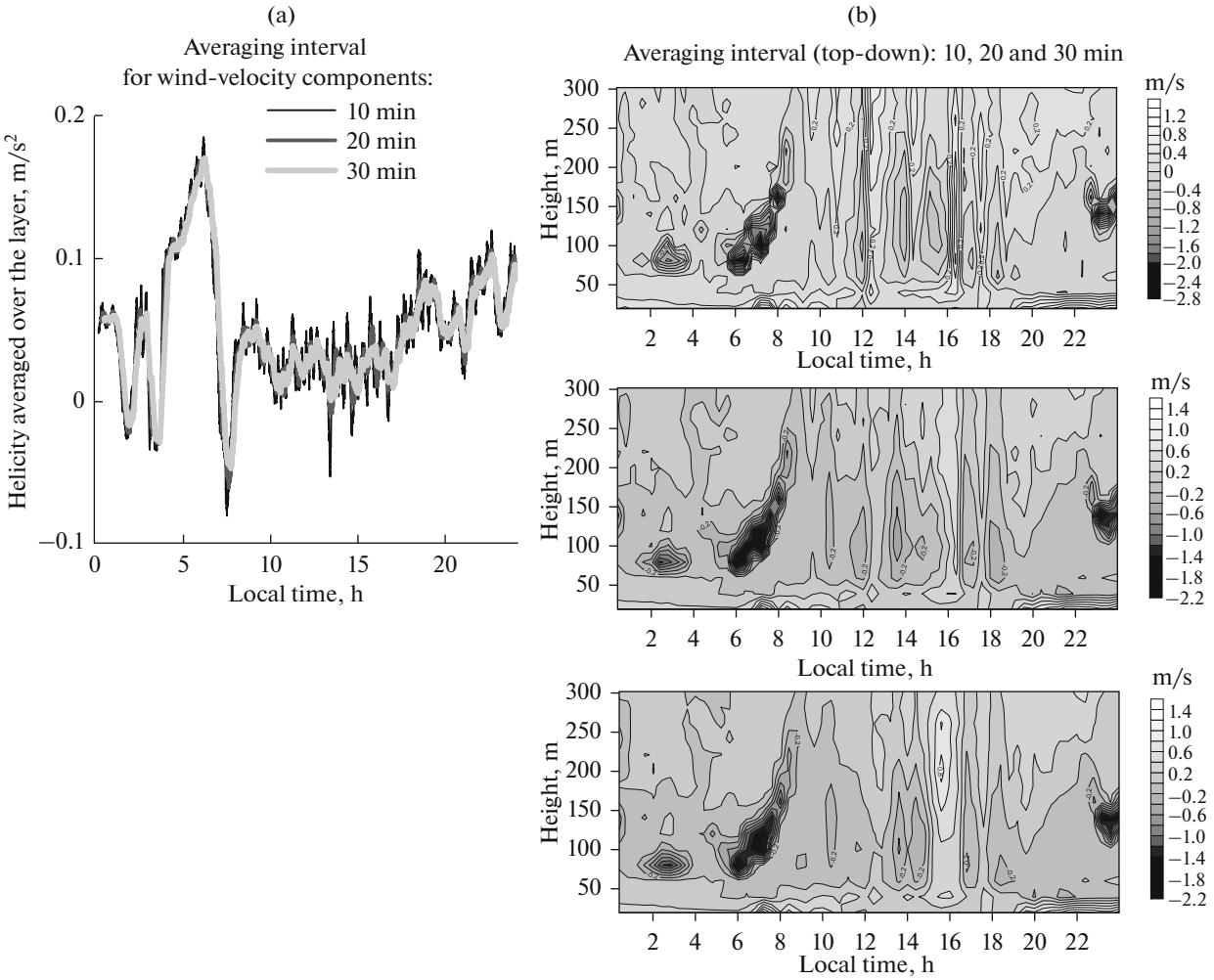

Fig. 1. Time variations in (a) helicity averaged over the layer and (b) vertical wind-velocity component in relation to averaging interval for wind velocity components (Kalmykia, July 25, 2007).

adequately illustrate the alternating stages of stable and unstable stratifications. For stable stratification, the vertical velocity at the boundary-layer height changes its sign. During the measurements taken on the island of Spitsbergen, stable stratification was observed.

3. DATA TREATMENT AND SIMULATION METHODS

Available data make it possible to calculate only horizontal helicity components. It should be noted that, under ordinary conditions, the main contribution to helicity is made by its horizontal component, which is, in particular, determining for a mesoscale roll circulation in the ABL [9, 31]. In this case, the vertical component of helicity is 5–10 times smaller than its horizontal component, because the former is determined by the product of vertical velocity and horizontal shear, which is significantly smaller than the vertical one (see, for example, table in [31]). This is also supported by observed values of the vertical component of turbulent helicity in the ABL [13, 14], which is evidently associated with its values for large-scale motions. Below, helicity will imply its horizontal component calculated according to (3).

Note that the vertical component of helicity is significant and exceeds its horizontal component for intense atmospheric vortices such as tornadoes and dust devils.

The wind-velocity components averaged are used to calculate helicity. To this end, a rectangular filter is used. The averaging interval was empirically chosen and, in this case, amounted to 10 min. At such values, the spatiotemporal velocity-field structure was adequately reproduced. On the basis of experimental data obtained in Kalmykia on July 25, 2007, Fig. 1 shows how the choice of averaging interval affects time variations in the averaged vertical component of wind velocity and averaged (over the layer) helicity.

Since wind-velocity profiles obtained with Doppler sodars remain sufficiently jagged even after averaging, then, in order to estimate the vertical derivatives of wind velocity, these profiles were smoothed out. They were approximated using cubic splines

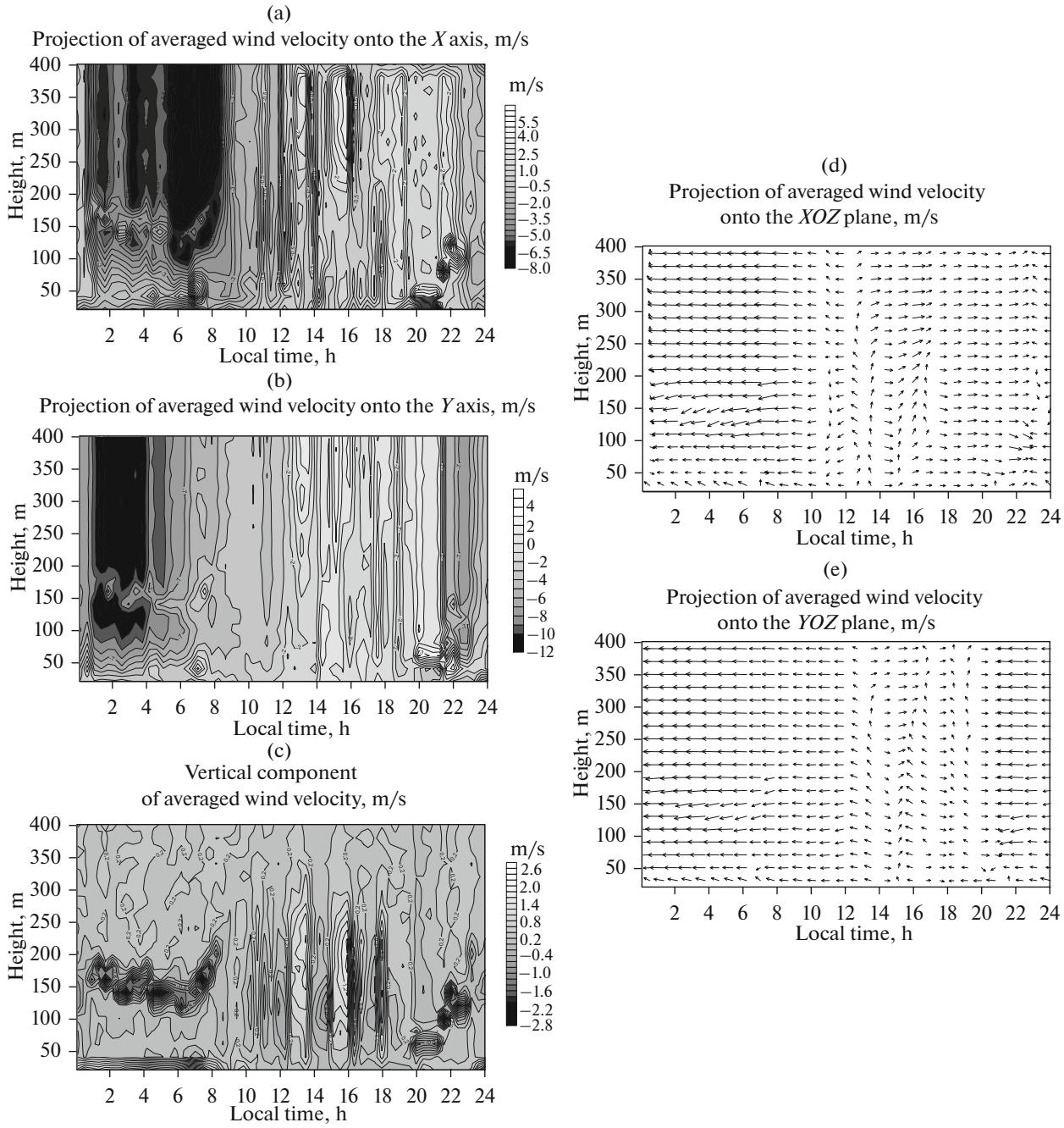

Fig. 2. Projections of averaged wind velocity onto the (a) *X*, (b) *Y*, and (c) *Z* axes and onto the (d) *XOZ* and (e) *YOZ* planes (Kalmykia, July 28, 2007).

with the following calculation of derivatives of already smoothed-out profiles.

The vertical components of wind velocity allow one to better (than its horizontal components) visualize structures observed in the ABL. Below, we will also use data vertical velocity component data. Thus, Fig. 2 shows the wind-velocity projections on axes Z, Y, and Z and velocity variations with height and time for July 28. Mesoscale structures start to form approximately at 12:00. This is also illustrated by a satellite image of the measurement region [3], in which the formation of cloud streets is observed: they start to form at 12:00 (local time) and these structures have already formed by 14:00 (local time).

4. SIMULATING AN OBSERVED SYNOPTIC SITUATION WITH A WRF MODEL

An open nonhydrostatic mesoscale model (Weather Research and Forecasting (WRF) model, version 3.6.1) was chosen to numerically simulate a synoptic situation observed during the experiment in

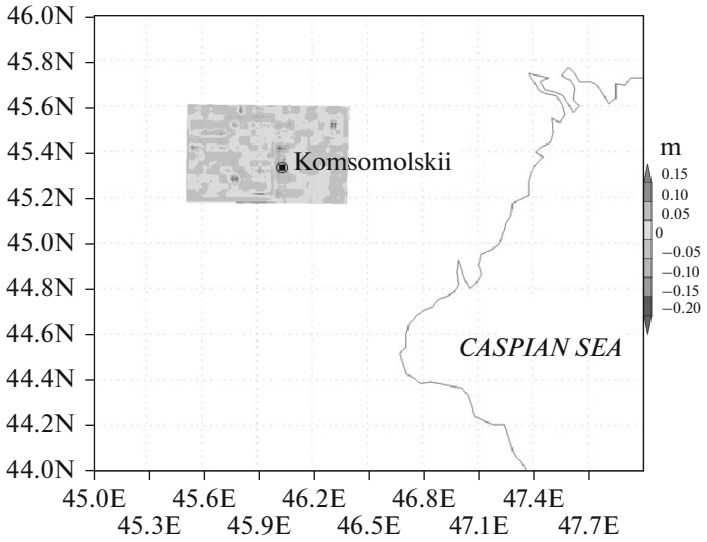

Fig. 3. Calculation area 300 by 225 km with the use of a coarse grid of 200 × 150 points horizontally with a step of 1500 m. The relief of the nested area is isolated.

Kalmykia [32, 33]. At present, the WRF model is one of the most universal and tuned-open systems of simulating the atmosphere. This model is successfully and widely used in meteorological forecasting and atmospheric research at scientific institutions and meteorological services in many countries and it is being continuously developed [34, 35].

The prognostic variables of the model are as follows: horizontal wind-velocity components u and v in the Cartesian coordinates, vertical velocity w, and both potential-temperature and geopotential disturbances. The geostrophic wind was determined according to these variables in order to calculate helicity.

Nested grids were used in calculations. The whole calculation area, 300 by 225 km, is calculated using a coarse grid of 200 × 150 points horizontally with a step of 1500 m. The nested area of detailed calculations 75 by 50 km, in which sodar data are assimilated, is calculated using a grid of 151 × 106 points with a step of 500 m (see Fig. 3). Both areas have 35 levels along the vertical up to a height of 5000 m, with their crowding within the boundary layer. Three calculation steps for the nested area correspond (in time) to one calculation step for the large area. The time interval between the initial fields of meteorological parameters of the operational Global Forecast System (GFS) analysis on a grid of 0.5° × 0.5° amounts to 6 h. The coordinates of the calculation-area center correspond to 45° N and 45° E. Note that the mesoscale circulation starts to be reproduced on grids with a horizontal scale of 500 m. Coherent vortex structures may reach 5 km in width, and ten points are sufficient to qualitatively reproduce mesoscale-circulation features. In this case, helicity was not calculated directly in the model; only the wind-velocity components and geopotential at the grid points were calculated for further calculation of the geostrophic wind-velocity components.

In order to increase the accuracy in forecasting atmospheric characteristics, surface measurement data on meteorological parameters were assimilated. Data obtained with the long-wave sodar located in Kalmykia on the northern outskirts of the village of Komsomolskii at the point with the coordinates 45.33527° E and 46.02687° N were used as assimilated data. Observational data were assimilated using a three-dimensional variational method based on the 3DVar system [36].

Data postprocessing was performed to obtain integral helicity. The components of geostrophic wind velocity at the point located at a distance of 3.5 km from the point of inputting assimilated data were determined through geopotential values calculated by the model. The following formulas were used:

$$U_G = -\frac{g}{2\Omega\sin(\varphi)}\frac{dh_g}{dy};\ U_a = U - U_G,$$

$$V_G = \frac{g}{2\Omega\sin(\varphi)}\frac{dh_g}{dx},\ V_a = V - V_G.$$

Here, U and V are the horizontal wind-velocity components, U_a and V_a are the ageostrophic wind-velocity components, $g = 9.81$ m/s^2 is the free fall acceleration, φ is the geographic latitude, h_g is geopotential, $dx = rd\theta\cos(\varphi)$, $dy = rd\varphi$, $r = 63.7 \times 10^6$ m is the Earth's radius, and θ is the geostrophic longitude.

In order to find the geostrophic wind velocity from the above formulas, it is necessary to specify the height at which the wind may be considered geostrophic. We specified this height as a height of minimum ageostrophic component [37].

The geostrophic wind-velocity components make it possible to estimate integral helicity and compare

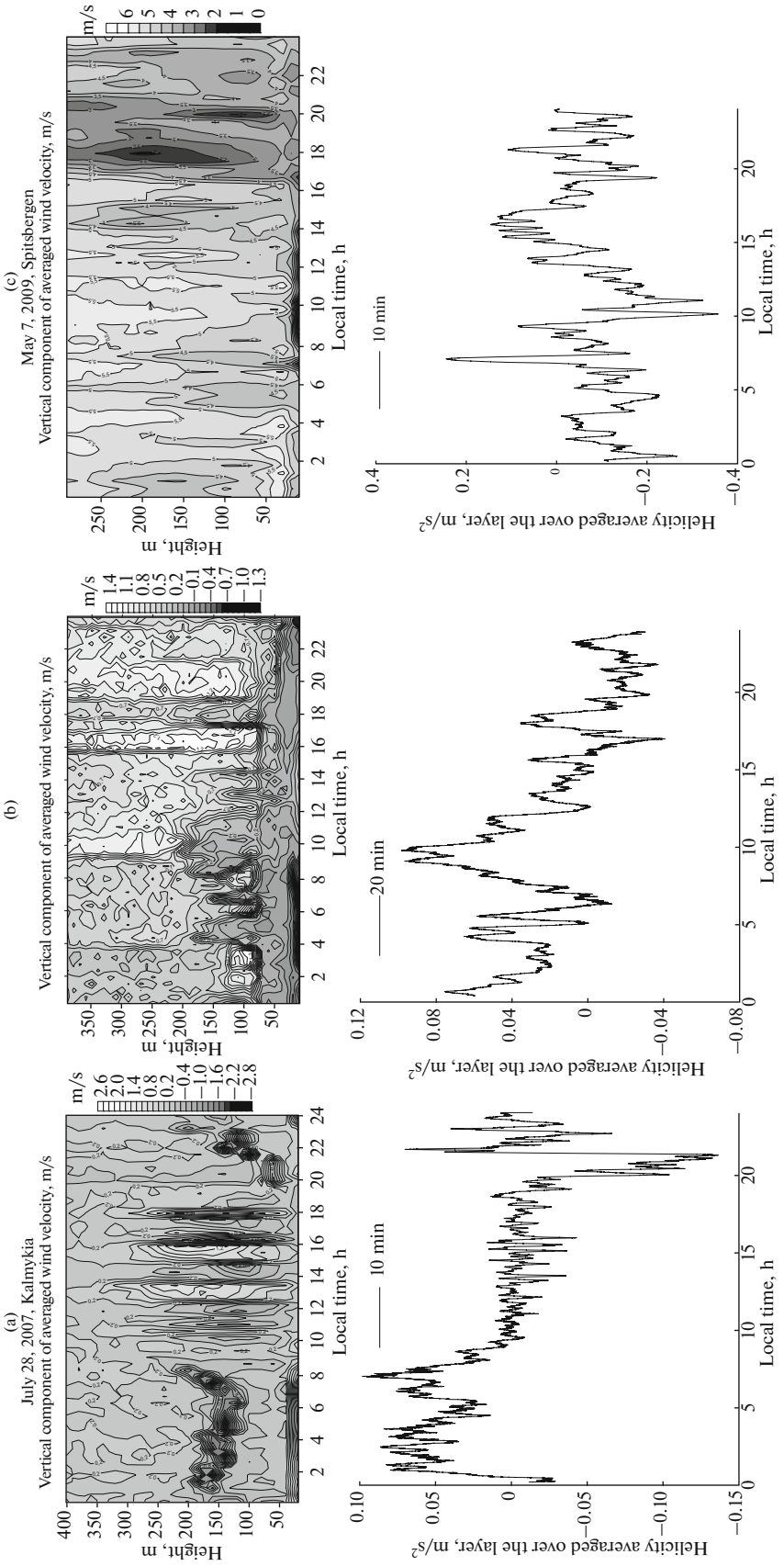

Fig. 4. Time variations in the height distribution of the averaged vertical wind-velocity component and helicity averaged over the layer for (a) Kalmykia, July 28, 2007; (b) Tsimlyansk, August 9, 2012; and (c) Spitsbergen, May 7, 2009. The averaging intervals for the wind-velocity components amounted to (a, c) 10 min and (b) 20 min.

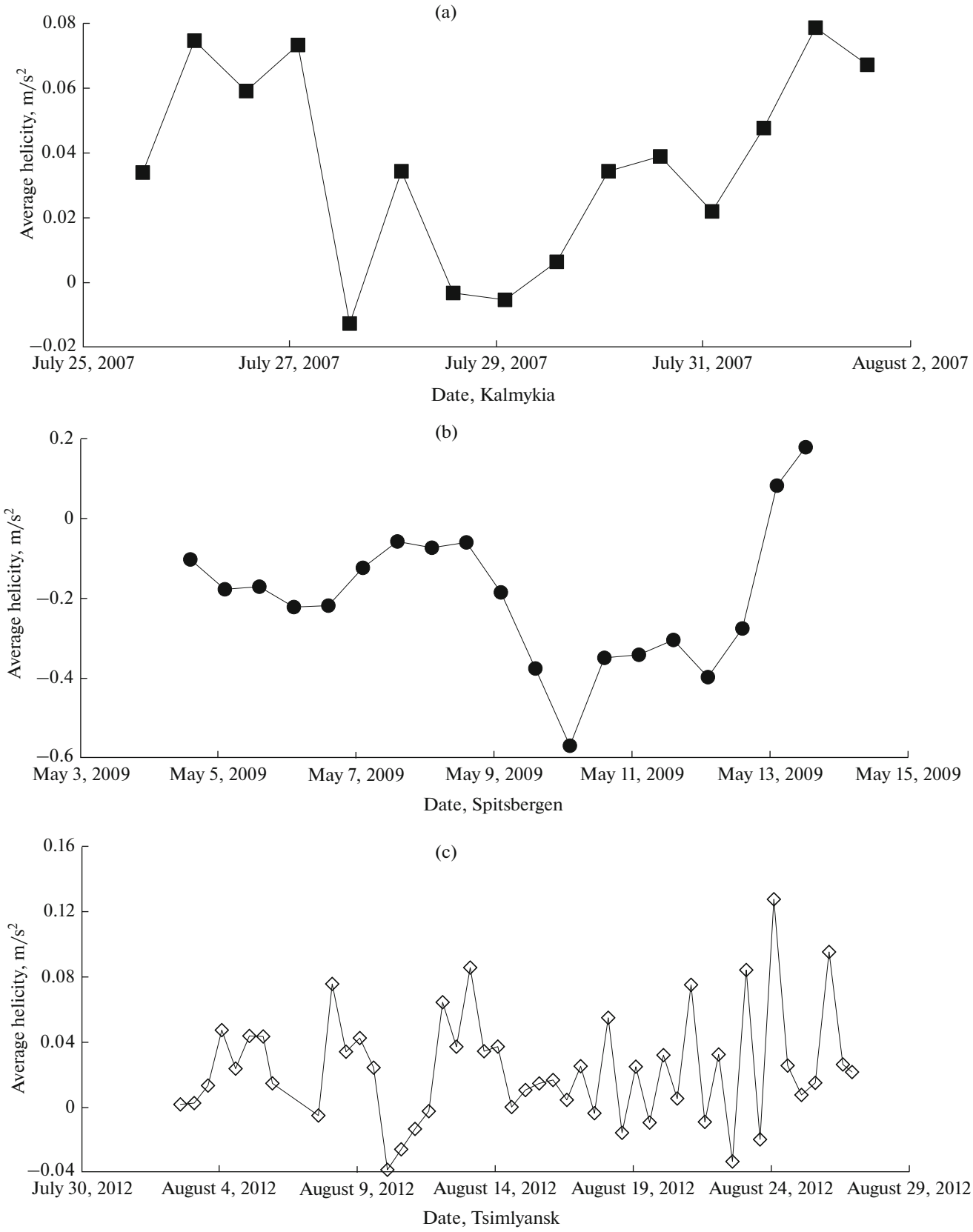

Fig. 5. Time variations in helicity with a 12-h averaging for (a) Kalmykia, (b) Spitsbergen, and (c) Tsimlyansk.

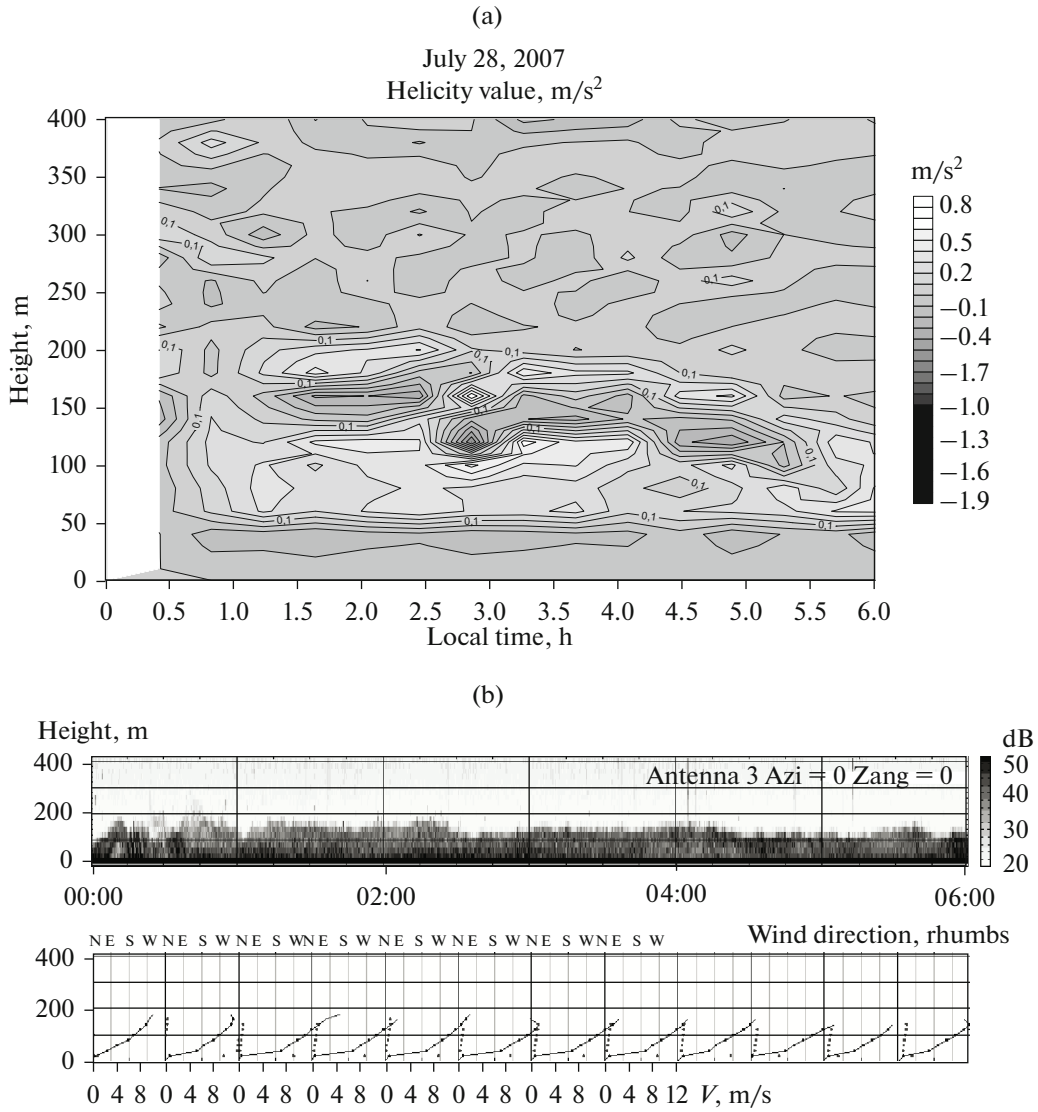

Fig. 6. Time variations in the height distribution of helicity and the echogram of the vertical wind-velocity component. Kalmykia, July 28, 2007, 00:00–06:00: (a) helicity values. (b) top: sodar echogram; the intensity of echo signal is given in dB. (b) bottom: the lines with dots—vertical profiles of the wind speed, dots without lines—profiles of the wind direction expressed in rhumbs. The dots on the curves correspond to the values with sufficient statistical reliability.

these estimates with its values obtained from acoustic sounding data.

5. RESULTS

The results of calculations of helicity according to acoustic sounding data establish its relation with wind velocity and ABL structures.

Under ordinary conditions, a major contribution to the ABL helicity is made by its horizontal components. This is also supported by turbulence data [13, 14]. Nevertheless, in a number of cases, a stable correlation is observed between the vertical wind-velocity component and helicity averaged over the layer, which is supported by the idealized theory of the Ekman boundary layer [17].

Figure 4 shows time variations in the distribution of the averaged vertical wind-velocity component and helicity averaged over the layer: (a) for July 28, 2007, Kamykia; (b) for August 9, 2012, Tsimlyansk Scientific Station; and (c) for May 7, 2009, Spitsbergen. In Fig. 4, one can see the vertical wind-velocity component extrema associated with developing large-scale coherent structures. Figure 5 shows time variations in helicity with a 12-h averaging.

Note that the formation of large-scale structures in the wind field is manifested in the vertical wind-velocity echogram and in the time variations in the height distribution of helicity. In Kalmykia, on July 26, 28, and 30 and August 1, 2007, low-level jet flows that are also well reflected in both the echogram and helicity distribution were observed at night (see Fig. 6 for July 28).

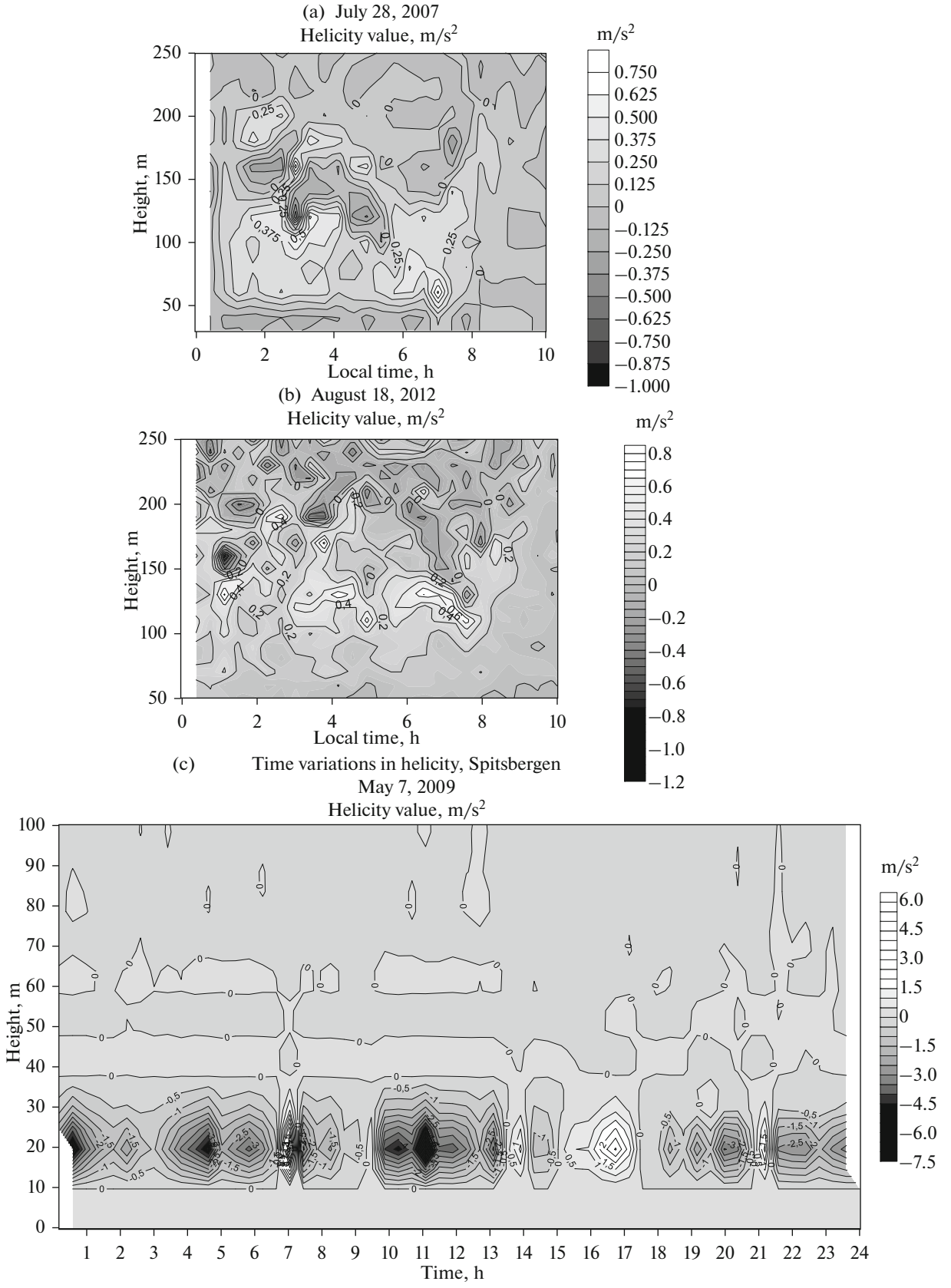

Fig. 7. Helicity for night jet flows in (a) Kalmykia, July 28, 2007, and (b) Tsimlyansk, August 18, 2012; (c) time helicity variations on May 7, 2009, Spitsbergen.

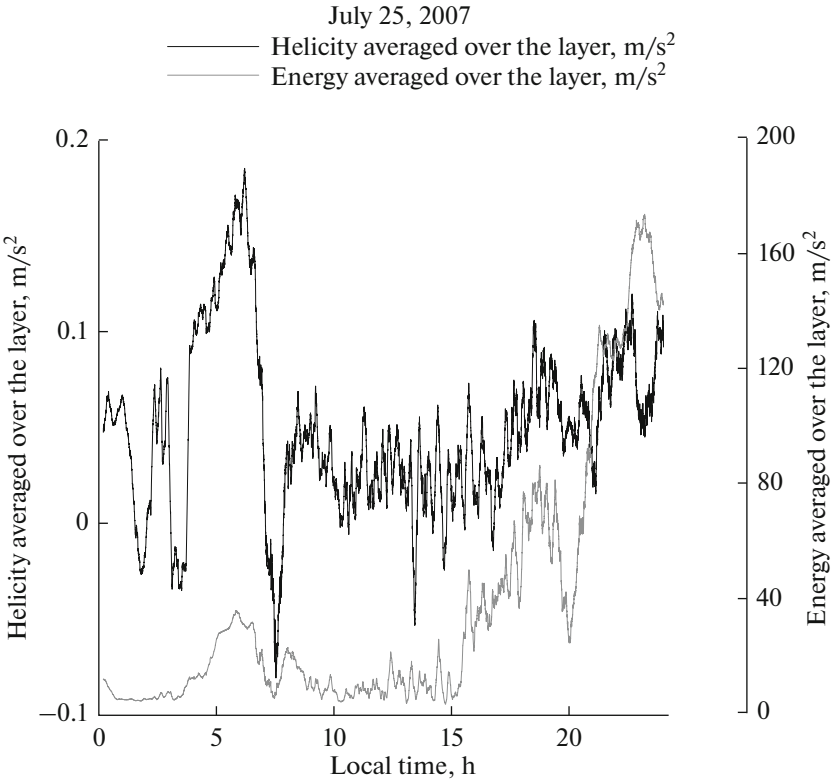

Fig. 8. Relation between helicity averaged over the layer and specific kinetic energy for July 25, 2007, Kalmykia. The values of helicity averaged over the layer are multiplied by 200 for more convenient comparison.

The vertical wind-velocity profiles in the echogram, which characterize the night jet flows, correspond to a maximum increase in helicity reflected in the time profile of its height distribution. There are also some examples of night jet flows observed on August 11 and 18, 2012, at the Tsimlyansk Scientific Station. In this case, a noticeable increase in helicity (when compared to its daytime values) should be noted (see also [38]). Helicity reaches 0.8 m/s^2 (see Figs. 7a and 7b for Kalmykia, July 28, and Tsimlyansk, August 18).

For Spitsbergen, the formation of structures in the ABL wind-velocity field occurs at a height of up to 50 m, which is characteristic of the polar latitudes (see Fig. 7c). In most cases, the reliability of data is limited to a height of approximately 100 m because of a high level of acoustical noise generated by the the wind.

The mean values of helicity for large-scale motions amount to 0.3–0.6 m/s^2; they exceed its independently measured turbulent values by an order of magnitude [13, 14, 39].

There is good relation between helicity averaged over the layer and energy—the sum of the squared velocities of all three wind components (see Fig. 8).

Note that the experimental values of helicity averaged over the layer are close to theoretical values of turbulent helicity and amount to approximately 0.02–0.12 m/s^2.

The possibility of using Eq. (4) in an idealized Ekman model and in estimating integral helicity has been studied. The results given in Fig. 9 show a good correlation between integral helicity (H_{int} (3)) calculated through the integration of (3) and the half-sum of squared geostrophic-wind components (H_{int}); for the Ekman boundary layer, the relation between these two quantities was first noted in [10]. The correlation coefficients for Kalmykia and Tsimlyansk are calculated for each case and are close to one. Figure 9 shows the results for July 29, 30, and 31, 2007, Kalmykia: $r_{29} = 0.7234$, $r_{30} = 0.6717$, and $r_{31} = 0.7722$, as well as for August 4, 9, and 15, 2012, Tsimlyansk: $r_{4\ 08:00-16:00} = 0.7887$, $r_{9\ 00:00-02:00} = 0.9121$, $r_{9\ 09:00-16:00} = 0.9325$, and $r_{15\ 12:00-21:00} = 0.7189$.

Integral helicity calculated from Eq. (4) is compared to that calculated using the WRF model. Figure 10 shows the sample results for July 29, 2007. On the whole, the results of calculations with sodar-data assimilation are closer to helicity values assessed earlier, when compared with the results of calculations without sodar-data assimilation.

CONCLUSIONS

In this work, on the basis of data obtained from the acoustic sounding of the ABL in the three IAP field

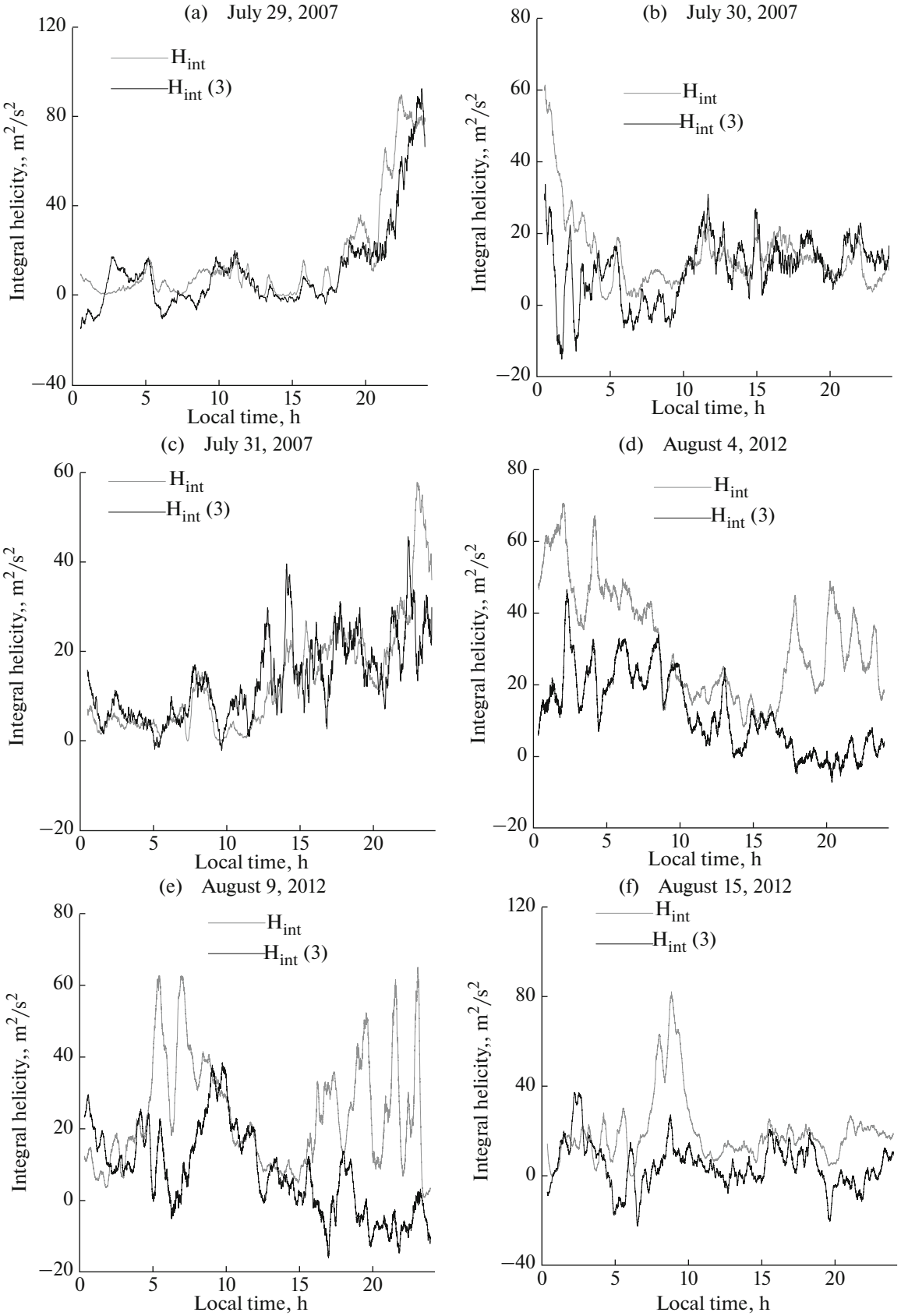

Fig. 9. Relation between integral helicity H_{int} (3) and the sum of squared geostrophic velocity components H_{int} for (a) July 29, (b) July 30, and (c) July 31, 2007, Kalmykia, and (d) August 4, (e) August 9, and (f) August 15, 2012, Tsimlyansk.

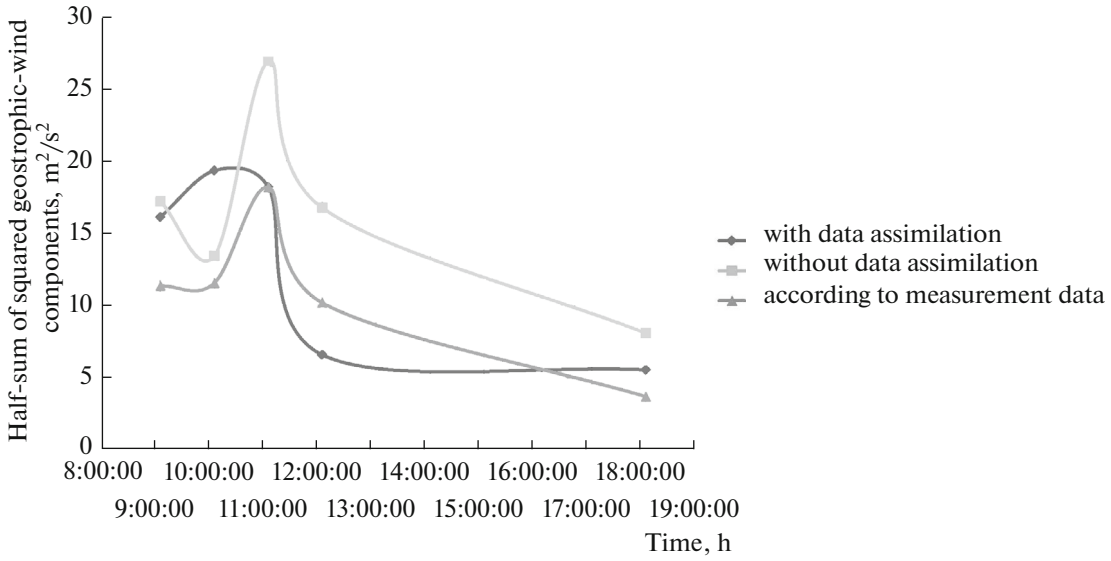

Fig. 10. Results of calculations with the WRF model. Comparison of half-sums of squared geostrophic velocity components, Kalmykia, July 29, 2007.

experiments, the absolute helicity of large-scale motions and the helicity averaged over the layer were estimated at 0.3–0.6 and 0.02–0.12 m/s^2, respectively. Based on data on velocity gradients and known Reynolds shear stress values, one can estimate coefficients of a semiempirical turbulence model with the parameterization of turbulent helicity [12, 18].

The relation between helicity averaged over the layer and kinetic energy is shown.

In the absence of strong convection, there is good correlation between variations in integral helicity and those in squared wind velocity at upper sounding levels (400–600 m), which (under these conditions) may replace (with an adequate accuracy) squared geostrophic-wind velocity variations. This makes it possible to simplify the construction of both global and regional helicity fields, in particular, in solving prognostic problems. Empirical values of integral helicity were verified using the WRF open nonhydrostatic mesoscale atmospheric model with assimilated acoustic sounding data.

ACKNOWLEDGMENTS

We thank M.V. Kurgansky and L.O. Maksimenkov for their helpful remarks and interest in our work. The research was supported by the Russian Scientific Fund (project no. 14-27-00134). The in-field measurements, processing of the data were supported by the Russian Foundation for Basic Research (projects no. 12-05-10043-к, 13-05-00846). The numerical simulation was supported by the Russian Foundation for Basic Research (project no. 14-05-00847).

REFERENCES

1. P. Markovski and Y. Richardson, *Mesoscale Meteorology in Midlatitude* (John Wiley and Sons, Chichester, 2010).
2. N. F. Vel'tishchev and V. M. Stepanenko, *Mesometeorological Processes. A Textbook* (MGU, Moscow, 2006).
3. I. G. Granberg, V. F. Kramar, R. D. Kuznetsov, O. G. Chkhetiani, M. A. Kallistratova, S. N. Kulichkov, M. S. Artamonova, D. D. Kuznetsov, V. G. Perepelkin, V. V. Perepelkin, and F. A. Pogarskii, "A study of the spatial structure of the atmospheric boundary layer with a Doppler-sodar network," Izv., Atmos. Ocean. Phys. **45** (5), pp. 541–548 (2009).
4. D. Etling and R. A. Brown, "Roll vortices in the planetary boundary layer. A review," Boundary-Layer Meteorol. **65**, 215–248 (1993).
5. S.-H. Chou and M. P. Ferguson, "Heat fluxes and roll circulations over the western Gulf Stream during an intense cold-air outbreak," Boundary-Layer Meteorol. **55** (3), 255–281 (1991).
6. J. Wurman and J. Winslow, "Intense sub-kilometer-scale boundary layer rolls observed in Hurricane Fran," Science **280** (5363), 555–557 (1998).
7. H. Morrison, J. A. Curry, and V. I. Khvorostyanov, "A new double-moment microphysics parameterization for application in cloud and climate models. Part I: Description," J. Atmos. Sci. **62** (6), 1665–1677 (2005).
8. M. V. Kurgansky, Introduction to large-scale atmospheric dynamics (Adiabatic invariants and their use) (Gidrometeoizdat, St. Petersburg, 1993) [In Russian].
9. D. Etling, "Some aspect of helicity in atmospheric flows," Beitr. Phys. Atmos. **58** (1), 88–100 (1985).
10. M. V. Kurgansky, "Relationship between helicity and potential vorticity in a compressible rotating fluid," Izv.

Akad. Nauk, Fiz. Atmos. Okeana **25** (12), 979–981 (1989).

11. R. Hide, "Superhelicity, helicity and potential vorticity," Geophys. Astrophys. Fluid Dyn. **48** (1–3), 69–79 (1989).
12. O. G. Chkhetiani, "On the helical structure of the Ekman boundary layer," Izv., Atmos Ocean. Phys. **37**(5), 569–575 (2001).
13. B. M. Koprov, V. M. Koprov, V. M. Ponomarev, and O. G. Chkhetiani, "Experimental studies of turbulent helicity and its spectrum in the atmospheric boundary layer," Dokl. Phys. **50** (8), 419–422 (2005).
14. B. M. Koprov, V. M. Koprov, M. V. Kurgansky, and O. G. Chkhetiani, "Helicity and potential vorticity in surface turbulence," Izv., Atmos. Ocean. Phys. **51** (6), 565–575 (2015).
15. E. Deusebio and E. Lindborg, "Helicity in the Ekman boundary layer," J. Fluid Mech. **755**, 654–671 (2014).
16. M. V. Kurgansky, "Helicity in dynamic atmospheric processes," Izv., Atmos. Ocean. Phys. **53** (2) 127–141 (2017).
17. V. M. Ponomarev and O. G. Chkhetiani, "Semiempirical model of the atmospheric boundary layer with parametrization of turbulent helicity effect," Izv., Atmos Ocean. Phys. **41** (4), 418–432 (2005).
18. H. Pichler and A. Schaffhauser, "The synoptic meaning of helicity," Meteorol. Atmos. Phys. **66**, 23–34 (1998).
19. I. A. Repina, B. V. Ivanov, and R. D. Kuznetsov, "Measurement of the katabatic wind turbulent structure in the Spitsbergen coastal zone," Sovrem. Probl. Distantsionnogo Zondirovaniya Zemli Kosmosa, No. 2, 180–188 (2009).
20. R. A. Brown, *Analytical Methods in Planetary Boundary-Layer Modeling* (New York, Wiley, 1974; Gidrometeoizdat, Leningrad, 1978).
21. N. L. Byzova, V. N. Ivanov, and E. K. Garger, *Turbulence in the Atmospheric Boundary Layer* (Gidrometeoizdat, Leningrad, 1989) [In Russian].
22. G. I. Taylor, "Eddy motion in the atmosphere," Philos. Trans. R. Soc. London **215**, 523–537 (1915).
23. M. A. Kallistratova, R. D. Kuznetsov, and I. V. Petenko, "The implementation of A.M. Obukhov's idea on ground-based remote sensing of the lower troposphere by acoustic and electromagnetic waves," in *Turbulence, Dynamics of the Atmosphere and Climate: Proceedings of the International Conference in Commemoration of Academician A. M. Obukhov (May 13–16, 2013)*, Ed. by G. S. Golitsyn, I. I. Mokhov, S. N. Kulichkov, M. V. Kurgansky, and O. G. Chkhetiani (GEOS, Moscow, 2014), pp. 593–620 [in Russian].
24. G. H. Crescenti, "A look back on two decades of doppler sodar comparison studies," Bull. Am. Meteorol. Soc. **78**, 651–673 (1997).
25. R. L. Coulter and M. A. Kallistratova, "The role of acoustic sounding in a high technology era," Meteorol. Atmos. Phys. **71**, 3–13 (1999).
26. S. Emeis, *Surface-Based Remote Sensing of the Atmospheric Boundary Layer* (Springer, 2011), Chap. 3. doi 10.1007/978-90-481-9340-0
27. P. S. Anderson, R. S. Ladkin, and I. A. Renfrew, "An autonomous Doppler sodar wind profiling system," J. Atmos. Oceanic Technol. **22**, 1309–1325 (2005).
28. M. A. Kallistratova, R. D. Kouznetsov, V. F. Kramar, and D. D. Kuznetsov, "Profiles of vertical wind speed variances within nocturnal low-level jets observed with a sodar," J. Atmos. Oceanic Technol. **30**, 1970–1977. doi 10.1175/JTECH-D-12-00265.1
29. R. D. Kuznetsov, "Acoustic sounder LATAN-3 for studies of the atmospheric boundary layer," Opt. Atmos. Okeana **20** (8), 749–753 (2007).
30. R. D. Kouznetsov, "The multi-frequency sodar with high temporal resolution," Meteorol. Z. **18** (2), 169–173 (2009).
31. R. Cieszelski, "Studies on turbulence parametrizations for flows with helicity," Izv., Atmos Ocean. Phys. **35** (2), 157–170 (1999).
32. W. C. Skamarock, J. B. Klemp, I. Dudhia, et al., *A Description of the Advanced Research WRF Version 3*, NCAR Tech. Note 475, June 2008.
33. N. F. Vel'tishchev and V. D. Zhupanov, *Numerical Weather Predictions with WRF-ARW and WRF-NMM Nonhydrostatic Models in General Use* (TRIADA, Moscow, 2010), pp. 94–135 [In Russian].
34. E. V. Nabokova, "Attempt of WRF model application with two methods of urban layer parameterization for the prediction of air temperature and wind velocity," in *Transactions of the Hydrometeorological Center of the Russian Federation, Atmospheric Physics and Weather Forecast* (GMTs RF, Moscow, 2010), No. 344, 180–195 [In Russian].
35. K. G. Rubinshtein, E. V. Nabokova, R. Yu. Ignatov, M. M. Smirnova, R. V. Arutyunyan, V. N. Semenov, O. S. Sorokovikova, and A. V. Fokin, "Influence of parameterization methods for boundary layer processes in the WRF model on the prediction of wind velocity and the results of admixture transport simulation," *Transactions of the Hydrometeorological Center of the Russian Federation, Atmospheric Physics and Weather Forecast* (GMTs RF, Moscow, 2010), No. 344, pp. 196–213 [In Russian].
36. D. M. Barker, W. Huang, Y. R. Guo, and Q. N. Xiao, "System for use with MM5: Implementation and initial results," Mon. Weather Rev., **132**, 897–914 (2004).
37. J. R. Holton, *An Introduction to Dynamic Meteorology* (Elsevier, Burlington, 2004).
38. R. A. Maddox, "Diurnal low-level wind oscillation and storm-relative helicity," in *The Tornado: Its Structure, Dynamics, Prediction, and Hazards* (AGU, Washington, D.C., 1993), pp. 591–598.
39. B. M. Koprov, V. M. Koprov, M. V. Kurgansky, and O. G. Chkhetiani, "Helicity of atmospheric turbulence," in *Turbulence and Wave Processes: Book of Abstracts of the International Conference in Commemoration of the Centenary of the Birth of M. D. Millionshchikov* (Intuit.ru, Moscow, 2013), pp. 26–28.

Translated by B. Dribinskaya